

12. CYCLIC SEDIMENTATION AT SITES 745 AND 746¹

Werner U. Ehrmann² and Hannes Grobe²

ABSTRACT

The upper Miocene to Pleistocene sediments recovered at ODP Sites 745 and 746 in the Australian-Antarctic Basin are characterized by cyclic facies changes. Sedimentological investigations of a detailed Quaternary section reveal that facies A is dominated by a high content of siliceous microfossils, a relatively low terrigenous sediment content, an ice-rafted component, low concentrations of fine sediment particles, and a relatively high smectite content. This facies corresponds to interglacial sedimentary conditions. Facies B, in contrast, is characteristic of glacial conditions and is dominated by a large amount of terrigenous material and a smaller opaline component. There is also a prominent ice-rafted component. The microfossils commonly are reworked and broken. The clay mineral assemblages show higher proportions of glacially derived illite and chlorite.

A combination of four different processes, attributed to glacial-interglacial cycles, was responsible for the cyclic facies changes during Quaternary time: transport by gravity, ice, and current and changes in primary productivity. Of great importance was the movement of the grounding line of the ice shelves, which directly influenced the intensity of ice rafting and of gravitational sediment transport to the deep sea. The extension of the ice shelves was also responsible for the generation of cold and erosive Antarctic Bottom Water, which controlled the grain-size distribution, particularly of the fine fraction, in the investigated area.

INTRODUCTION

Ocean Drilling Program (ODP) Leg 119 Sites 745 (59°35.710' S, 85°51.600' E) and 746 (59°32.8235' S, 85°51.780' E) were drilled in water depths of 4082 and 4059 m, respectively (Fig. 1). The aim was to obtain a deep-water Neogene reference section that could be compared with the sections in shallow and intermediate water depths drilled on the Kerguelen Plateau previously on Leg 119 (Sites 736, 737, 738, and 744) and later during Leg 120 (Sites 747-751). Sites 745 and 746 are about 5.5 km apart within the Australian-Antarctic Basin, just east of the steep southeastern flank of the Kerguelen Plateau. They are beneath the present-day Antarctic Bottom Water (AABW; Emery and Meincke, 1986).

Both sites were drilled near the crest of the East Kerguelen Ridge (Houtz et al., 1977). This large sedimentary ridge is morphologically and seismically similar to sediment drifts. It parallels the eastern flank of the Kerguelen Plateau, from which it is separated by a depression about 10 km wide, for about 550 km. At the site locations, the ridge crest rises about 400 m above the surrounding deep-sea floor. Seismic investigations indicate that the sediment distribution is influenced by currents (Barron, Larsen, et al., 1989).

The upper Miocene to Quaternary sedimentary sequence recovered at Sites 745 and 746 has a pelagic, mixed biogenic siliceous and terrigenous character. It consists almost entirely of alternating clayey diatom oozes and diatomaceous clays (Ehrmann et al., this volume). In this paper the two main lithologies have been defined as facies A (clayey diatom ooze) and facies B (diatomaceous clay).

Cyclic changes of sedimentary facies are well known in Pleistocene sediments from the Antarctic continental margin in the eastern Weddell Sea (Grobe, 1986; Grobe et al., 1990). The sediment composition in this area is also characterized by significant changes in the content of ice-rafted debris, grain-size distribution,

clay mineral assemblage, and biogenic components. The depositional environment is controlled mainly by ice rafting and bottom current transport, whereas primary productivity is influenced by the sea ice coverage and thus reflects the glacial-interglacial cycles in detail. The influence of different bottom water current velocities on the grain-size distribution was observed, for example, in the northeastern part of the Weddell Sea (Fütterer et al., 1988; Pudsey et al., 1988). The flow of Weddell Sea Bottom Water is documented along the continental slope off the South Orkney Plateau as a contour current forming erosional channel structures. This current is responsible for changes in grain-size composition that can also be correlated with the climatic cycles (Fütterer et al., 1988).

The objectives of our sedimentological analyses were to determine the effects of AABW on sediment composition and depositional environment during the Quaternary. Interest was concentrated mainly on the source of the detrital sediment component and the mode of its transportation and accumulation. One possibility would be that the Kerguelen Plateau supplied sediment to the sites by downslope movement. However, sediment could result from northward transport by bottom currents from the Antarctic continental margin. In the latter case, the cyclic facies changes possibly would reflect glacial-interglacial cycles controlling the supply of fine- and coarse-grained material.

During glacial periods, the movement of the ice shelf and thus of the grounding line reaching the shelf break, as reported from Prydz Bay for several Cenozoic time intervals, may have delivered terrigenous material to the continental slope (Grobe, 1986; Kellogg and Kellogg, 1988; Vorren et al., 1988; Hambrey et al., this volume). The finer material was brought in suspension by major gravitational transport processes, such as sediment gravity flows, and then redistributed by currents. In contrast, during interglacial periods this material may have been deposited on the shelf, without being affected significantly by currents. Other possibilities are that sedimentation was exclusively controlled by fluctuations in the production of siliceous organisms in the surface water and their preservation in the sediment, by a changing ratio between bottom current activity and intensity of ice rafting according to the glacial-interglacial cycles, or by combinations of any of these possibilities.

¹ Barron, J., Larsen, B., et al., 1991. *Proc. ODP, Sci. Results*, 119: College Station, TX (Ocean Drilling Program).

² Alfred Wegener Institute for Polar and Marine Research, Columbusstraße, D 2850 Bremerhaven, FRG.

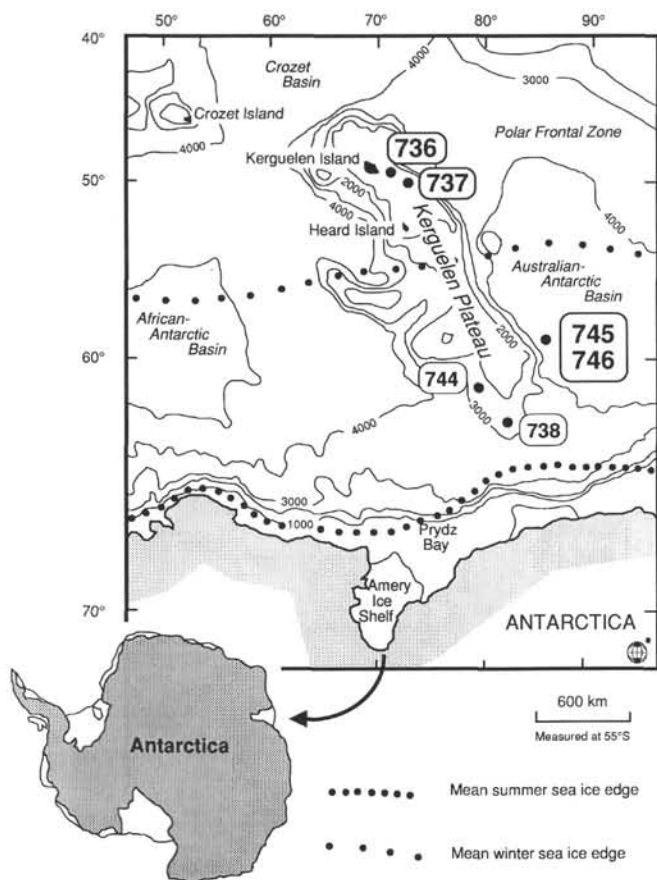


Figure 1. Location map of ODP Leg 119 Sites 745 and 746. Bathymetry (in meters) is from GEBCO (Hayes and Vogel, 1981; Fisher et al., 1982). The position of the Polar Front is according to Whitworth (1988), the mean sea ice cover in summer and winter according to Dietrich and Ulrich (1968).

METHODS

Samples were taken at 8–35-cm intervals from a detailed interval at Site 745 (Sections 119-745B-7H-2 to 119-745B-7H-5) from 54.0 to 59.3 m below seafloor (mbsf). Sample size was 3–5 cm³. Due to pressure release during the retrieval of the drill cores from a water depth of about 4000 m, recovery often exceeded 100%. Depth information in this paper is corrected for core recoveries > 100%.

Carbonate and Organic Carbon

Total carbon content and carbonate-bound carbon were determined on freeze-dried and ground bulk samples using a Coulomat 702 (Ströhlein Instruments). Total carbon was set free by heating the sample to 1100°C. Carbonate-bound carbon was released by treatment with 14% phosphoric acid. Organic carbon and carbonate (CaCO₃) contents were calculated as weight percent.

Grain Size

Bulk samples disaggregated by freeze-drying and subsequent treatment with 10% H₂O₂ were washed through 2-mm and 63- μ m sieves to isolate the gravel and sand fractions. The clay fraction (< 2 μ m) was separated from the < 63- μ m fraction by decantation (settling time based on Stokes' law). In order to remove the biogenic opaline components from the terrigenous sedimentary particles, such as quartz, feldspar, and rock frag-

ments, a density separation was performed on the sand and silt fractions. A sodium-polytungstate solution was used as heavy liquid, with its density adjusted to 2.3 g/cm³. The separation was carried out in a centrifuge. Amorphous silica (mainly diatom debris) was removed from the < 2- μ m fraction by a 3-min treatment with a boiling 2 M Na₂CO₃ leach.

The grain-size distribution of the terrigenous silt fraction (2–63 μ m) was analyzed using a particle-size analyzer SediGraph 5000ET (Micromeritics). Grain sizes were calculated individually for the bulk sediment, terrigenous components, and opaline components. Statistical grain-size parameters (Folk and Ward, 1957; Folk, 1966) were calculated for the terrigenous fraction.

Clay Mineralogy

The clay mineral composition was analyzed by X-ray diffraction (XRD) of the opal-free < 2- μ m fraction. All samples were washed free of salt and decalcified. The samples were fixed as texturally oriented aggregates on aluminium sample holders and solvated with 60°C warm ethylene-glycol vapor for about 18 hr immediately before the analyses. The measurements were conducted on an automated powder diffractometer system PW 1700 (Philips) with CoK α radiation (40 kV, 40 mA), graphite monochromator, automatic divergence slit, and an automatic sample changer.

The samples were X-rayed from 2°–40° 2 θ with a speed of 0.02° 2 θ /s. Individual clay minerals were identified by their basal reflections at 15–18 Å (smectite), 10 Å (illite), 7 and 3.57 Å (kaolinite), and 14.2, 7, 4.72, and 3.54 Å (chlorite). Semiquantitative evaluations of the clay mineral assemblage used empirically estimated correction factors on integrated peak areas of the individual clay mineral reflections from the glycolated samples (Biscaye, 1964, 1965; Lange, 1982).

Bulk Mineralogy

XRD analyses were also performed on bulk sediment samples. They were freeze-dried and then ground in an agate mortar. A mixture of 200 mg of sample and 100 mg of an internal standard (Al₂O₃) was pressed as randomly oriented slides in aluminium sample holders. The quartz content was calculated using a specific standard curve. Relative changes in the concentrations of other minerals present in the samples were detected by the mineral/standard peak height or area ratios.

Roundness

The roundness of quartz grains in the sand fraction was determined visually using comparative images (Pettijohn, 1975).

NATURE OF THE SEDIMENTARY CYCLES

As well as showing differences in composition, the diatomaceous clays (facies B) are slightly darker than the clayey diatom oozes (facies A). The differences, however, are so subtle that most of them did not result in different color codes from the Munsell Soil Color Chart. The colors in the investigated interval range from greenish gray (5GY 5/1) to dark gray (5Y 4/1). All transitions are very diffuse. Facies B intervals generally have a cut surface with a smoother texture than that of the facies A intervals. Both lithologies are homogeneous and do not show significant internal structures. According to the core descriptions (Barron, Larsen, et al., 1989), bioturbation does not play an important role. The boundaries between adjacent facies are mostly gradational over several centimeters to decimeters or diffuse. In only a few cases were sharp lower boundaries observed in facies B. Erosional contacts, however, could not be proved. Facies B intervals are typically 0.1 to 1 m thick; 167 of them were identified at Sites 745 and 746 (Ehrmann et al., this volume).

In order to investigate the differences in the sediment composition between facies A and facies B in more detail and to

gain information on the origin of the cyclic sedimentation, a 5.3-m interval from Site 745 was sampled and analyzed. This interval contains three facies B intervals (Fig. 2). The boundaries with facies A intervals are distinct, with the exception of a diffuse and bioturbated transition at 59.0 mbsf.

Stratigraphically, the detailed section represents part of Quaternary time (Barron, Larsen, et al., 1989). According to paleomagnetic data (H. Sakai, pers. comm., 1989; Baldauf and Barron, this volume), the base of the Jaramillo Event (0.98 Ma; Berggren et al., 1985) is at 54.3 mbsf, and the average sedimentation rate is estimated as about 5 cm/1000 yr. The 5.3-m-thick section investigated therefore embraces a time span of about 100,000 yr. Unfortunately, the age control is not sufficient to calculate accumulation rates for the individual facies A and B intervals.

General Sediment Composition

The opaline sediment component of both facies consists mainly of diatoms. Radiolarians, silicoflagellates, and sponge spicules occur in lesser amounts. The total opal content is 40%–60% in facies A and 10%–35% in facies B (Fig. 2).

Carbonate occurs as microcarbonate, because no foraminifers were detected with the optical microscope. The carbonate content is relatively constant and low, exceeding 0.5% in only a few samples (Fig. 2). It does not reflect the cyclic sedimentation pattern. The highest values, however, occur within facies A, a feature that also can be seen in the long-term record of Sites 745 and 746 (Ehrmann et al., this volume). The maximum concentrations seem to occur at the base of facies A intervals. The car-

bonate content of 7.5% in Sample 119-745B-7H-3, 26–27 cm, represents the highest value recorded in samples from Sites 745 and 746, although higher values were found in an isolated thin nannofossil ooze layer at Site 746 (246.7–247.3 mbsf; Ehrmann et al., this volume). The content of organic carbon fluctuates between 0.1% and 0.2% without any correlation with facies changes (Fig. 2).

Because carbonate is a minor sediment component and has little influence on the bulk sediment composition, opaline and terrigenous material are the main sedimentary constituents and are strongly inversely correlated (Fig. 2). According to XRD and microscopic investigations the terrigenous material consists of quartz, alkali feldspar, plagioclase, and minor amounts of amphibole and accessory minerals. As expected, quartz content correlates with the amount of terrigenous material and is highest in facies B. However, it does not exceed 12%. Because feldspar cannot be easily quantified, an XRD quartz/feldspar ratio was calculated (Fig. 2). The ratio increases slightly upcore and shows only minor fluctuations. Its trend is similar to the concentrations of quartz and total terrigenous material and lacks significant shifts that could be related to lithologic changes.

Grain Size

As the two facies are characterized by different amounts of clay and silt-size diatoms, the changes in lithology are well documented in the grain-size distribution of the bulk sediment (Fig. 3). Opaline particles occur mostly within the 2–63- μ m fraction, but minor proportions also occur in the >63- μ m fraction and as broken frustules in the <2- μ m fraction. It is obvious that

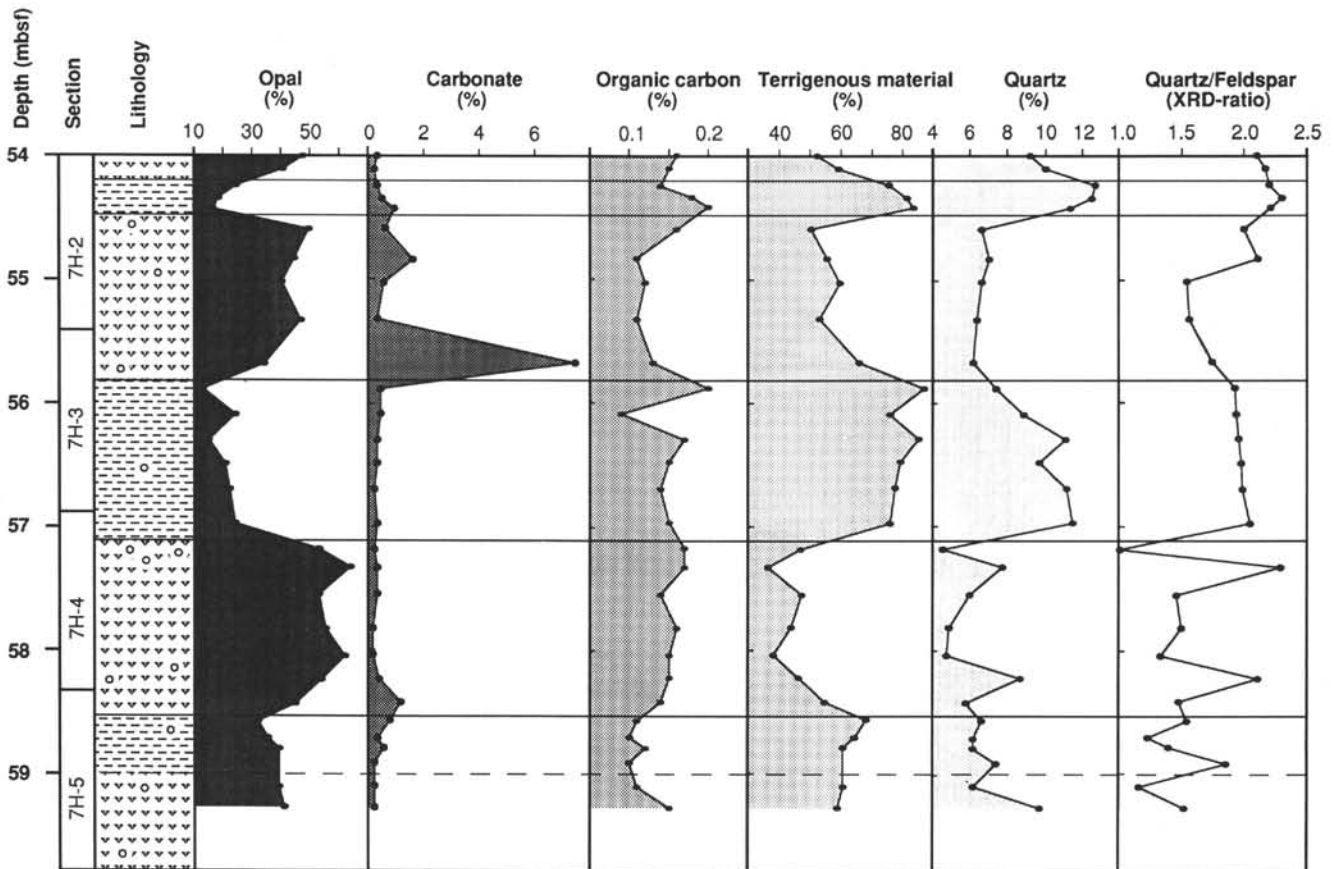


Figure 2. Sediment composition in an interval from Hole 745B. The lithology column indicates the cyclic alternations of facies A (clayey diatom ooze) and facies B (diatomaceous clay) and the occurrence of ice-rafted pebbles and granules (see Fig. 4). Data are given in weight percent, except for the quartz/feldspar in XRD peak-area ratios (Appendix Table 1).

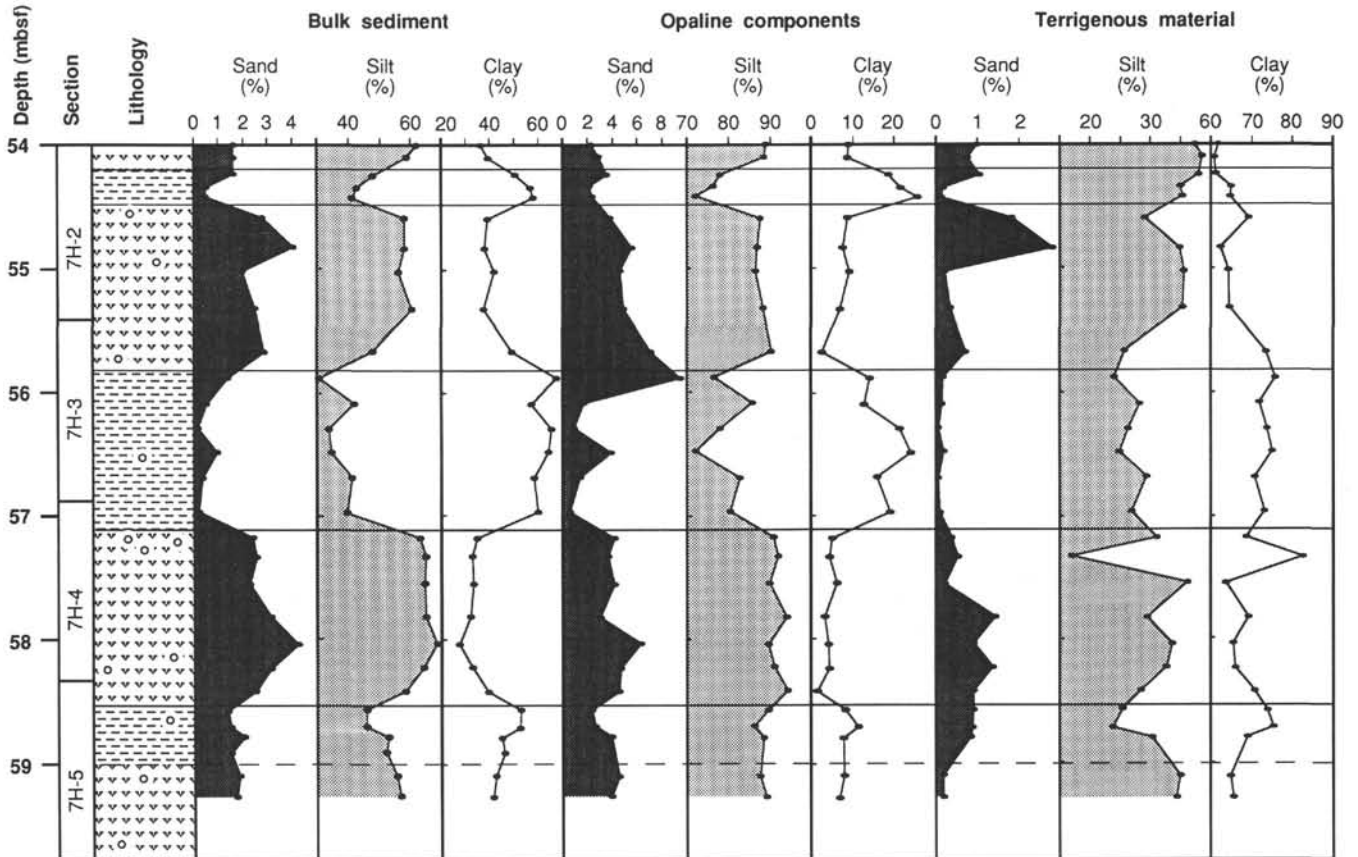


Figure 3. Grain-size distribution in an interval from Hole 745B. The grain size of the opaline and terrigenous sediment components is in percent of the individual component (Appendix Table 2). For example, opaline sand, silt, and clay add to 100%. Dilution effects arising from enhanced influx of the respective other components are thus excluded. See Figure 4 for the lithology column legend.

there is an enrichment of fine opaline fragments in facies B and an enrichment of the larger valves in facies A (Fig. 3).

The grain-size distributions of terrigenous matter do not show such clear patterns as do the opaline components. However, there is a tendency for facies A to be slightly enriched in coarser particles, even if the individual grain-size classes only poorly reflect the facies changes (Fig. 3). This is confirmed by the detailed grain-size distribution of the terrigenous silt fraction, which shows a roughly higher concentration of coarse silt in facies A than in facies B.

The terrigenous sand component is most abundant in facies A but is not totally absent from facies B. It appears that the highest terrigenous sand concentration occurs close to the transition between the two facies. Also, the long-term record (Ehrmann et al., this volume) reveals that terrigenous sand, as well as gravel, is not restricted to one facies.

Statistical treatment of the grain-size data was made for the terrigenous components (Fig. 4). Both the mean and the median sizes (Appendix Table 3) tend to show lower ϕ values (coarser size) in facies A. The sorting coefficient ranges from 1.8ϕ to 2.3ϕ , documenting typically poor to very poor sorting (Folk and Ward, 1957; Folk, 1966) of the terrigenous portion of the glaciomarine sediment. Sorting is better in facies B than in facies A.

The skewness coefficient is a measure of the asymmetry in the size distribution of particles in a sediment (Pettijohn et al., 1987). The coefficient is negative throughout (-0.5 to -0.3 ; i.e., the grain sizes on the fine side are cut off). There is a tendency toward stronger negative values in facies A (Fig. 4).

Kurtosis is a measure of the deviation of a grain-size distribution from a log normal distribution (e.g., Pettijohn et al., 1987). Normal curves have a kurtosis of 1.0. Values >1.0 indicate better sorting in the central part, and values <1.0 indicate better sorting in the tails. In the detailed interval from Site 745, the kurtosis ranges from 0.7 to 1.2, with low values occurring predominantly in facies A.

Clay Mineralogy

The clay mineral assemblage consists of smectite, chlorite, illite, and kaolinite (Fig. 5). Chlorite and illite are derived mainly from the physical weathering of crystalline and metamorphic rocks and are especially common in marine sediments at high latitudes (Biscaye, 1965; Griffin et al., 1968). Higher amounts of kaolinite normally are restricted to tropical regions with intense chemical weathering and soil formation on land. In Prydz Bay and on the southern Kerguelen Plateau, however, the clay mineral assemblage can be ascribed to erosion of old kaolinite-bearing sediments on the Antarctic continent (Ehrmann, this volume). Smectite is derived mostly from submarine chemical weathering of volcanic material (Biscaye, 1965).

The total amount of clay minerals (Fig. 5) represents the nonbiogenic $<2\text{-}\mu\text{m}$ fraction of the sediment. Concentrations range from 25% to 65%, with the lowest found in facies A. The concentration of individual clay minerals (Fig. 5) is given as a percentage of the clay mineral fraction (Biscaye, 1964, 1965). The assemblage is clearly dominated by illite (40%–70%). Smectite is present in concentrations of 10%–45%, and chlorite in concentrations of generally 10%–20%. Kaolinite is less impor-

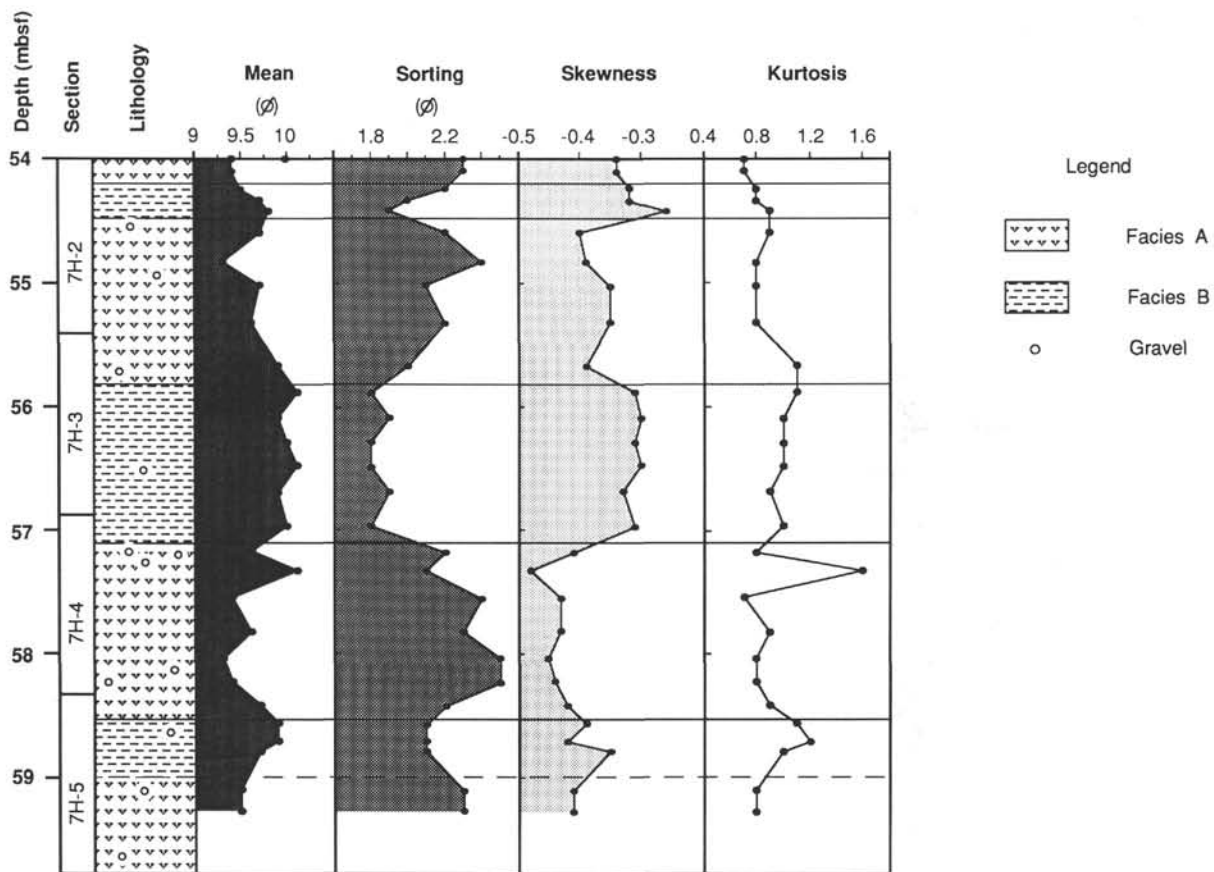


Figure 4. Statistical grain-size parameters (Folk and Ward, 1957; Folk, 1966) of the terrigenous material from an interval of Hole 745B (Appendix Table 3).

tant and accounts for mainly <10%, but up to 20%; minimum values occur in facies A. The highest smectite content is found in sediments where the total amount of clay minerals is low, corresponding mostly with facies A, even if that correlation in some places (e.g., at about 58 mbsf) is not very sharp. There is no correlation between the individual clay minerals other than that between smectite and illite.

Composition of the Terrigenous Sand Fraction

The nonbiogenic sand fraction (>63 μm) of the sediments does not show any major compositional changes. The quartz and feldspar content is very homogeneous (Fig. 6), and therefore the quartz/feldspar ratio, as a measure of transport wear, is also relatively constant. Along with these two minerals, amphibole and/or pyroxene occur in amounts of up to 8%. Accessory minerals garnet, glauconite, and mica are also present. All rock fragments are of gneissic or granitic composition. Their concentrations range from 1% to 9%, with peak values found in facies B.

Well-rounded sand-sized quartz grains are rare to absent in samples from the interval investigated, never exceeding 1.3%. Rounded grains normally range from 0% to 4%, with only two samples showing a higher proportion. Subrounded quartz grains occur in concentrations of about 20%. Most of the quartz sand grains (about 70%) belong to the subangular class. Angular grains comprise up to 10% (Fig. 6), indicating that most of the grains show little or no evidence of abrasion. It is clear that there is little variability in the roundness of the sand-sized quartz grains and that the fluctuations cannot be related to lithologic facies changes.

ORIGIN OF THE SEDIMENTARY CYCLES

Productivity

One way to explain the cyclic changes from diatomaceous clays to clayey diatom oozes as investigated at ODP Site 745 is to attribute them to dilution effects. It is possible that terrigenous material accumulated at a constant rate, while at certain times there was enhanced productivity and/or preservation of biosiliceous skeletons, resulting in higher biosiliceous accumulation rates.

The distribution of plankton in the surface waters, amongst other factors, is strongly dependent upon water temperature, nutrient availability, and light conditions. The productivity of the surface water and the composition of the sediments deposited beneath it are controlled mainly by the Polar Front, which represents a major water mass boundary separating the cold Antarctic Surface Water to the south from the warmer Subantarctic Surface Water to the north (Gordon, 1971). The position of the Polar Front is controlled by global climatic change. At present, it is at about 45°–50°S and lies close to the Kerguelen Plateau (Whitworth, 1988), about 1000 km north of Sites 745 and 746 (Fig. 1). However, in the region of the Kerguelen Plateau, the position of the Polar Front is highly variable. Thus, Deacon (1983) found a southward bend of this oceanographic boundary between Kerguelen Island and Heard Island. Surface sediments south of the Polar Front are dominated by biogenic siliceous sediments, and those close to the continent, by glaciomarine sediments with a dominant terrigenous component. North of the Polar Front biogenic calcareous sediments predominate.

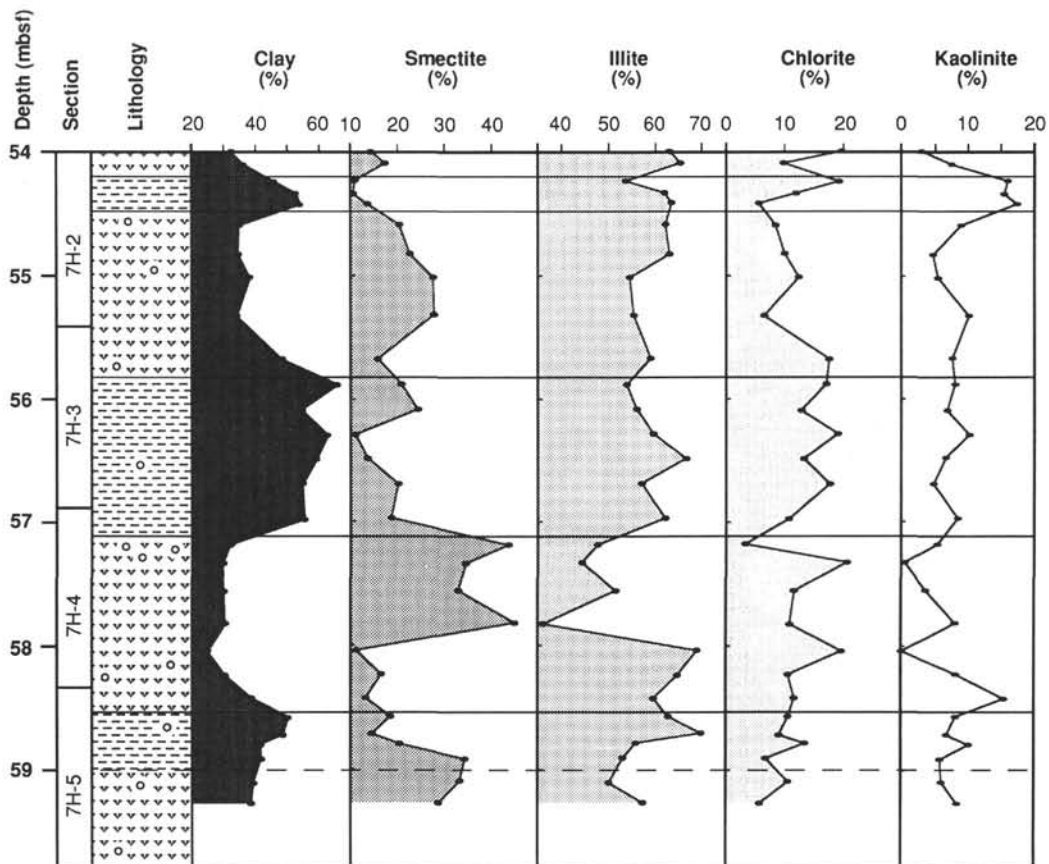


Figure 5. Amount of terrigenous clay (nonbiogenic, $<2 \mu\text{m}$) and relative percentages of the individual clay minerals smectite, illite, chlorite, and kaolinite in an interval from Hole 745B (Appendix Table 4). See Figure 4 for the lithology column legend.

The sea ice cover of the Southern Ocean is also controlled by climatic variations and the position of the Polar Front. Sea ice plays an important role in productivity, sedimentation processes, and stability in the water columns. It varies seasonally, as well as according to the long-term climatic fluctuations represented by glacial-interglacial cycles (Cooke and Hays, 1982; Burckle and Cooke, 1983; Burckle, 1984). In the present-day Indian Ocean close to Kerguelen Plateau, the sea ice reaches as far north as about 53°S during the winter season, whereas in summer it is restricted to south of about 64.5°S (Dietrich and Ulrich, 1968). Thus, fluctuations in the position of the Polar Frontal Zone and/or of the sea-ice cover, and thus of the belt of high productivity around Antarctica, may be responsible for the fluctuating opal content observed in the sediments of Sites 745 and 746.

In facies B intervals the diatom species *Eucampia antarctica*, which has been shown to be more abundant in South Atlantic sediments within upper Quaternary glacial intervals containing increased ice-rafted detritus (Burckle and Cooke, 1983), is more abundant than in facies A. Facies A, in contrast, contains species typical of interglacial periods. Glacial-interglacial cycles can also be recognized in the fluctuations of the radiolarian *Theocalyptra davisi* (Barron, Larsen, et al., 1989; Leg 119 Scientific Party, 1988). Interglacial periods are generally characterized by higher productivity because of the reduced sea-ice coverage and by the better preservation of opal in the sediment (Grobe et al., 1990).

The water depth at Sites 745 and 746 exceeds the carbonate critical depth ($<10\%$ CaCO_3 , about 3900 m; Kolla et al.,

1976a) but is less than the carbonate compensation depth (about 5200 m; Van Andel, 1975). For this reason, and because the sites are far south of the Polar Front, the carbonate content is generally very low and relatively constant. Peak carbonate production occurred during times of enhanced opal accumulation.

Fluctuations in the grain-size distribution of both opaline and terrigenous material, as well as in the distribution of the clay mineral assemblages (see the preceding section), prove that the generation of the cycles cannot be explained exclusively by a simple dilution effect. Other processes, such as transport by bottom currents or downslope transport must have been involved.

Downslope Transport

During periods of more extensive glacierization, the Antarctic ice shelves become thicker and more extended than during interglacial periods, because they are stabilized by the continuous sea ice cover. As the sea level is lowered, the grounding line moves seaward and, in places, may reach the shelf break (Kellogg et al., 1979; Elverhøi, 1981; Grobe, 1986). On the shelf, terrigenous weathering products and biogenic sediment components can be eroded, reworked, and transported by the ice to the shelf break. Transportation to the deep sea becomes feasible through the action of bottom currents or turbidity currents or as a result of slumping. Melting icebergs can bring basal debris directly to the deep ocean. Sediment, which during interglacial times is trapped on the shelf in front of the grounding line, may be "bulldozed" to the continental slope or incorporated into the base of the glacier as it advances across the continental shelf (Anderson et al., 1980; Elverhøi and Roaldset, 1983; Grobe,

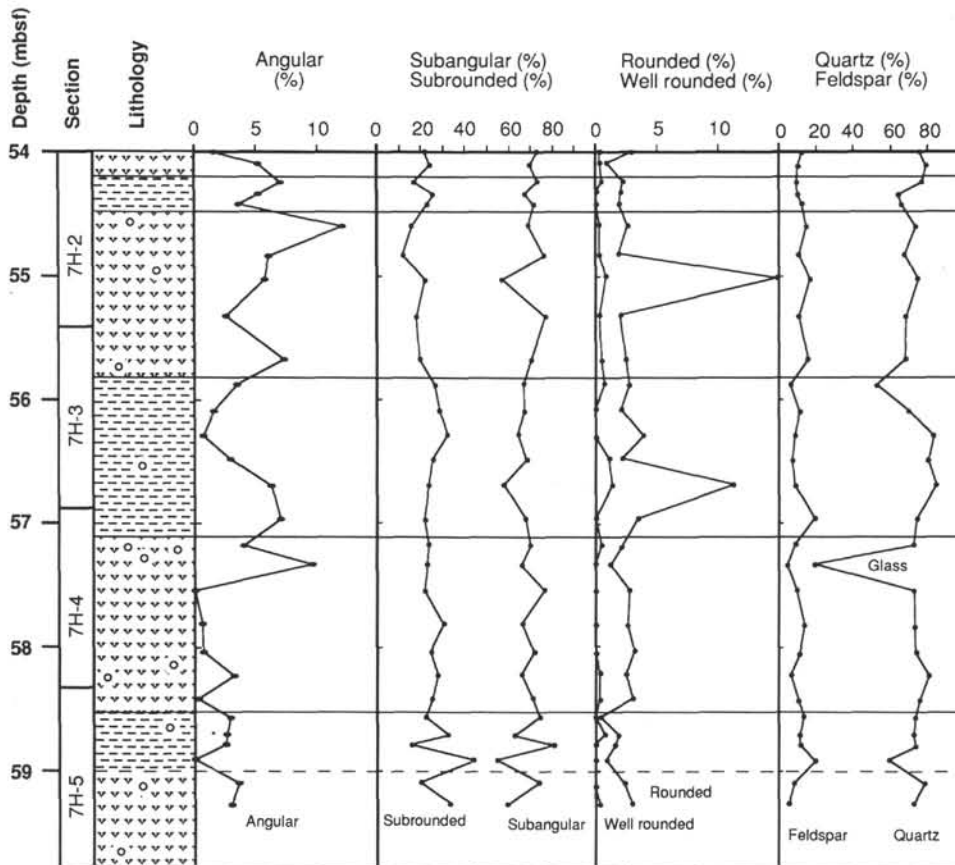


Figure 6. Roundness of quartz grains in the terrigenous sand fraction and concentrations of quartz and feldspar (by grain counts; Appendix Table 5). Roundness classes according to Pettijohn (1975). See Figure 4 for the lithology column legend.

1986; Vorren et al., 1988). The prograding sedimentary sequence on the Prydz Bay shelf may also be due to this process (Barron, Larsen, et al., 1989; Hambrey et al., this volume).

Downslope transport can explain the enhanced influx of terrigenous material during facies B glacial intervals. As for the opaline matter, the grain-size distribution of the terrigenous material also indicates that the fluctuations in the amount of this sediment component cannot be explained exclusively by dilution effects. During gravitational transport very slight sorting of the sediment load takes place as a result of the formation of turbidites (Fig. 4). Mainly the fine material reached Sites 745 and 746 as distal turbidites (Figs. 3 and 4), whereas the coarser material probably accumulated in the deep-sea basin closer to the continent or on the continental slope. Downslope transport also explains the greater importance of illite and chlorite, which are typical of physical weathering conditions on land. Illite and chlorite are probably delivered from the hinterland of the Prydz Bay area. The occurrence of broken opaline frustules in the $<2\text{-}\mu\text{m}$ fraction (Fig. 3) together with a peak occurrence of reworked radiolarians in facies B (J.-P. Caulet, pers. comm., 1988) is also due to these processes.

Eight thin silt layers were recorded at Site 745 (Barron, Larsen, et al., 1989). All but one of these occur within facies B. They are well sorted, have relatively sharp upper and lower contacts, and consist mainly of subangular to angular quartz and feldspar grains; fragmented diatom and spicule material is also present. Some of them are graded with heavy mineral concentrations at the base and some are laminated (Barron, Larsen, et

al., 1989). Thus, a turbiditic origin is probable, even if winnowing out of the finer material by currents cannot totally be ruled out for some of the silt layers. The turbidites might have been triggered by ice advances close to the shelf edge during low sea-level stands and/or by storms. This is consistent with the hypothesis that facies B accumulated during glacial periods.

Ice Rafting

The gravel content of sediments from Sites 745 and 746 indicates that ice rafting was an important factor, at least at certain times (Ehrmann et al., this volume). Although our samples did not contain gravel, some pebbles and granules were noted in the interval investigated (Figs. 2-6). The gravel, like the terrigenous sand, occurs in higher concentrations in facies A intervals.

Our investigations of the roundness of sand-sized quartz grains indicate that the grains experienced little abrasion and that there is no significant difference in abrasion between grains from the two facies. The quartz/feldspar ratio, an expected indicator for transport abrasion, is constant in both the bulk sediment and the sand fraction. For this reason, most of the sand is thought to have been brought to the site of deposition by ice rafting. Short-distance downslope transport of the sand fraction from the nearby continental slope, however, cannot be ruled out totally.

The general grain-size distribution of an ice-rafted sediment resembles that of a till, with all grain-size classes represented in roughly equal parts. While the larger particles quickly settle to the sea bed, the fine particles are prone to winnowing. How

much of the finer ice-rafted material is recorded in the sediment, therefore, is dependent on current velocities.

The Kerguelen Plateau is not a likely source of the sediment particles deposited at Sites 745 and 746. All the gravel and sand-size rock fragments are of gneissic or granitic character and resemble the rocks of the East Antarctic craton. Sedimentary clasts and basaltic components, which could have been derived from the plateau, are totally absent (Ehrmann et al., this volume).

Deep-Water Circulation

AABW, which today fills the Australian-Antarctic Basin (Fig. 1), is formed mainly along the Adélie Coast and in the Ross Sea (Jacobs et al., 1970; Eittrheim et al., 1972a, 1972b). It travels west, close to the Antarctic continent, until it hits the Kerguelen Plateau. There it is diverted to the north and flows parallel to the plateau (Kennett and Watkins, 1975, 1976; Kolla et al., 1976b). The AABW incorporated sedimentary particles that are suspended in the dense shelf water that sinks from the shelf break to the deep sea to form new AABW (Eittrheim et al., 1972b). AABW also interacts with the bottom sediment and may cause erosion. The sediment load, carried by the current, mostly settles out during its passage along the western side of the basin (Eittrheim et al., 1972a). It may thus be responsible for the East Kerguelen Ridge sediment drift, which is aligned parallel to the bottom current.

Seismic lines and 3.5-kHz records from Leg 119 confirm that currents influence the distribution of sediment. The top of the East Kerguelen Ridge has a wavy topography and the thicknesses of the sedimentary sequences are greatest on top of the ridge (where Sites 745 and 746 are situated) and on gentle slopes (Barron, Larsen, et al., 1989). Also, the relatively high number of older reworked diatoms and the occurrence of neritic and benthic diatoms throughout Sites 745 and 746 (J. Barron, pers. comm., 1989) provide evidence of bottom current activity.

Two mechanisms for the formation of bottom water have been discussed: deep convection in the open ocean triggered by increasing salinity in the surface waters during the formation of sea ice (Gordon, 1978, 1982; Killworth, 1979; Gordon and Huber, 1984) and mixing processes mainly off ice shelves and on continental slopes, as, for example, in the southern Weddell Sea (Foster and Carmack, 1976; Foster and Middleton, 1979; Foldvik et al., 1985; Foster et al., 1987). Ice Shelf Water, a major component in the formation of bottom water, is supposed to be formed under ice shelves (Hellmer, 1989).

As a result of the higher sea-level stand during interglacial periods, larger marginal parts of the Antarctic ice sheet are decoupled from the sea bed, which increases the size of the ice shelves. Water is able to flow beneath the ice and produce cold, dense Ice Shelf Water, which then mixes with Warm Deep Water and flows out over the shelf break into the deep ocean to form new AABW (Foldvik and Gammelsrød, 1988). Interglacial AABW circulation should therefore be stronger than during the glacial periods and increasing deep-sea erosion and transport of finer particles at the sediment/water interface by bottom currents would be expected. Even an increase in bottom water due to sea ice formation supports stronger current activities during interglacial periods, when sea ice is newly formed every season.

The sediment of facies A, which is thought to represent interglacial conditions, is depleted in the finer grain sizes of both terrigenous and opaline components. Despite winnowing, however, the terrigenous component of facies A does not become better sorted than the terrigenous material of facies B that is supplied by downslope transport.

CONCLUSIONS

A variety of sedimentary processes are responsible for the cyclic changes in lithology (Fig. 7) observed at Sites 745 and 746. All processes can ultimately be attributed to glacial-interglacial

cycles. Because the different processes interact in a complex way, the sedimentological parameters do not always mirror the climatic and environmental changes sharply. The contacts between the two principal lithologies are therefore mostly gradational. Bioturbation is only of minor importance.

Facies A consists of sediment deposited under interglacial conditions. It is dominated by siliceous microfossils and has a relatively low terrigenous sediment input, an ice-rafted component, a low concentration of fine sediment particles, and a higher smectite content.

During interglacial times the situation at the Antarctic continental margin resembled present-day conditions. Most of the terrigenous detritus carried by glaciers and ice shelves is melted out close to the grounding line or, in coastal regions without ice shelves, shortly after calving of icebergs (Drewry, 1986; Kellogg and Kellogg, 1988). This terrigenous sediment is mostly trapped on the continental shelf and slope (Fig. 7).

Productivity is relatively high during interglacial periods, and large amounts of diatoms and radiolarians accumulate near and south of the Polar Front. Bottom water circulation is stronger than in glacial periods because of the increased formation of cold and dense water beneath the Antarctic ice shelves, which is an important process in forming new AABW, possibly strengthened by the distinct seasonal variations in the formation of sea ice. Bottom currents at the sites winnowed out the finest sedimentary particles of terrigenous as well as biogenic origin, but were not strong enough to sort the terrigenous sediment components.

Ice rafting was active, especially during the transition from glacial to interglacial conditions. The decay of the ice shelves with rising sea level resulted in a large number of calving icebergs containing sediment at their base. Ice rafting decreased as soon as the grounding line reached its landward limit, and the decay of the ice shelves was completed (Grobe, 1986). At Sites 745 and 746, however, time resolution is not sufficient to reflect those processes in detail. Because downslope transport is not a major mechanism during interglacial periods, ice-rafted material dominates the terrigenous sediment components. Sorting of this material is very poor.

Facies B represents sediment typically deposited under glacial conditions (Fig. 7). It is dominated by terrigenous material and has a smaller opaline component. The microfossils commonly are reworked and broken. The clay mineral assemblages show a higher proportion of illite and chlorite, which are characteristic of physically weathered rocks of the East Antarctic craton and were probably reworked from the shelf area.

During glacial periods, the grounding lines of ice shelves moved seaward and stopped at or close to the shelf break. Shelf sediments were bulldozed over the shelf break and may have reached the deep ocean basins by gravitational transport processes. A certain amount of terrigenous weathering products rained out from melting icebergs directly onto the slope. Finer sediments on the slope could have been transported farther by currents. Sorting of the facies B terrigenous sedimentary component is poor to very poor, but slightly better than that of the predominantly ice-rafted terrigenous material of facies A.

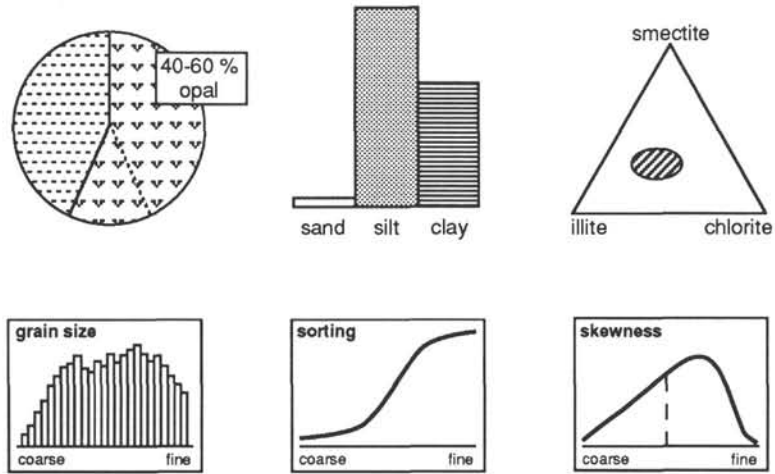
Once the formation of cold ice shelf water was reduced, AABW circulation became less erosive in character. Indications of turbidites, initiated by the advancing grounding line, may be seen in the few thin silt layers recovered at Site 745.

Productivity decreased during the transition from interglacial to glacial times, as recorded by a lower amount of siliceous microfossils in the sediments. The large and continuous extent of sea ice is responsible for low primary productivity as the light supply in surface waters is reduced (Grobe et al., 1990).

The diatom *Eucampia antarctica*, which is indicative of glacial conditions, is more abundant in the glacial facies B intervals than in the interglacial facies A intervals. Furthermore, the gla-

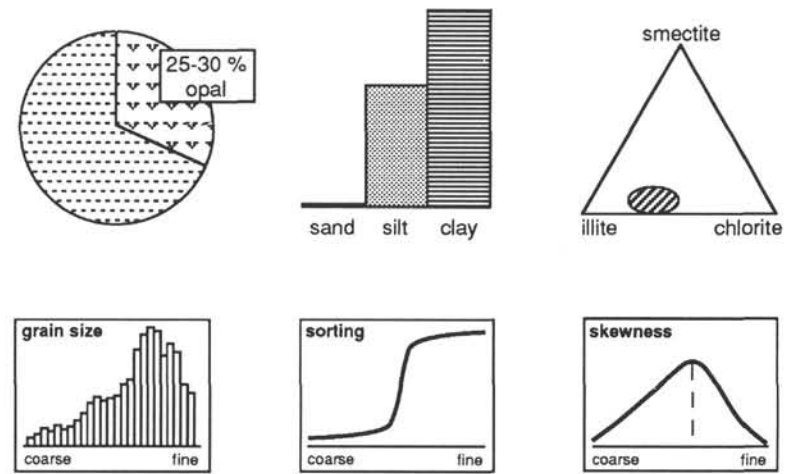
Facies A

clayey diatom ooze

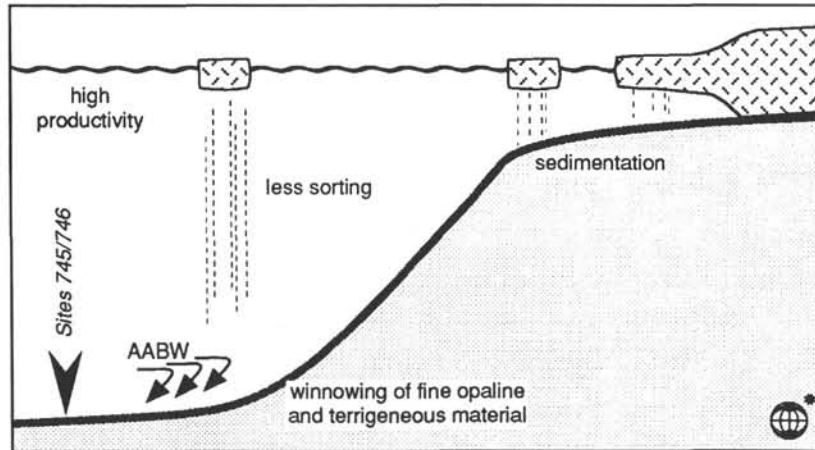


Facies B

diatomaceous clay



interglacial



glacial

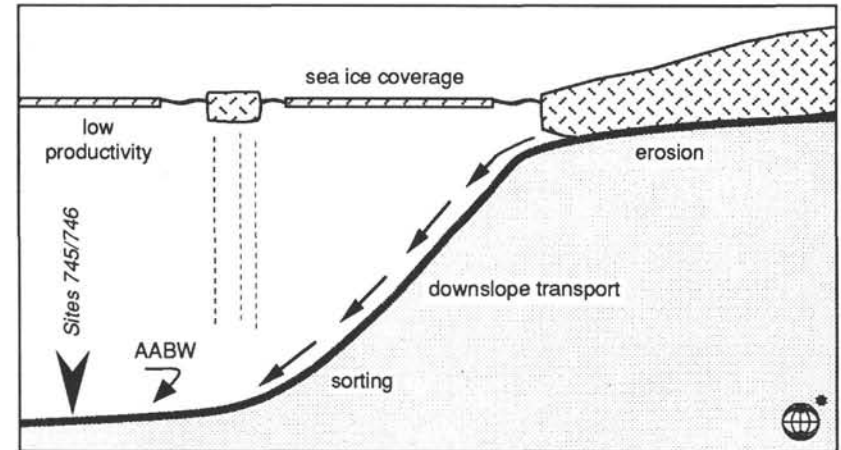


Figure 7. Simplified relative changes of some sediment parameters between the two main lithologies at ODP Sites 745 and 746 and a simplified model for the corresponding depositional environments. Grain size, sorting, and skewness data refer to the nonbiogenic material.

cial-interglacial cycles are mirrored in the abundance pattern of the radiolarian *Theocalyptra davisiana* (Barron, Larsen, et al., 1989).

Ice rafting was also active during glacial periods. Ice rafting seems to have been more intense during the transition from interglacial to glacial than during the glacial maxima, but less intensive than during the transition from the glacial to interglacial. Because ice shelves were grounded on the Antarctic continental shelves and because of the continuous sea ice cover during glacial maxima, relatively stable situations were established. These conditions reduced evaporation in the Southern Ocean and precipitation on the continent during glacial periods. Hence, the supply of snow was reduced and the mass balance of the ice sheets reduced. In addition, sea ice cover may have hampered icebergs from calving and drifting away (Grobe, 1986).

ACKNOWLEDGMENTS

The authors express their gratitude to M. Melles, G. Kuhn, and A. Mackensen for critical remarks and discussions. They further thank M. J. Hambrey for additional suggestions and correction of the English text. Laboratory work was assisted mainly by A. Hienen. This study was supported by grant Fu 119/15 of the Deutsche Forschungsgemeinschaft. This is Alfred Wegener Institute Contribution no. 273.

REFERENCES

- Anderson, J. B., Kurtz, D. D., Domack, E. W., and Balshaw, K. M., 1980. Glacial and glacial marine sediments of the Antarctic continental shelf. *J. Geol.*, 88:399-414.
- Barron, J., Larsen, B., et al., 1989. *Proc. ODP, Init. Repts.*, 119: College Station, TX (Ocean Drilling Program).
- Berggren, W. A., Kent, D. V., Flynn, J. J., and Van Couvering, J. A., 1985. Cenozoic geochronology. *Geol. Soc. Am. Bull.*, 96:1407-1418.
- Biscaye, P. E., 1964. Distinction between kaolinite and chlorite in recent sediments by X-ray diffraction. *Am. Miner.*, 49:1281-1289.
- , 1965. Mineralogy and sedimentation of recent deep-sea clays in the Atlantic Ocean and adjacent seas and oceans. *Geol. Soc. Am. Bull.*, 76:803-832.
- Burckle, L. H., 1984. Ecology and paleoecology of the marine diatom *Eucampia antarctica* (Castr.) Mangin. *Mar. Micropaleontol.*, 9:77-86.
- Burckle, L. H., and Cooke, D. W., 1983. Late Pleistocene *Eucampia antarctica* abundance stratigraphy in the Atlantic sector of the Southern Ocean. *Micropaleontology*, 29:6-10.
- Cooke, D. W., and Hays, J. D., 1982. Estimates of Antarctic Ocean seasonal sea-ice cover during glacial intervals. In Craddock, C. (Ed.), *Antarctic Geoscience*: Madison (Univ. Wisconsin Press): 1017-1025.
- Deacon, G.E.R., 1983. Kerguelen, antarctic and subantarctic. *Deep-Sea Res.*, Part A, 30:77-81.
- Dietrich, G., and Ulrich, J., 1968. *Atlas zur Ozeanographie*: Mannheim (Bibliographisches Institut).
- Drewry, D. J., 1986. *Glacial Geological Processes*: London (Arnold).
- Eitrem, S., Bruchhausen, P. M., and Ewing, M., 1972a. Vertical distribution of turbidity in the South Indian and South Australian Basins. *Antarct. Res. Ser.*, 19:51-58.
- Eitrem, S., Gordon, A. L., Ewing, M., Thorndike, E. M., and Bruchhausen, P., 1972b. The nepheloid layer and observed bottom currents in the Indian-Pacific Antarctic Sea. In Gordon, A. (Ed.), *Studies in Physical Oceanography*: New York (Gordon & Breach), 19-35.
- Elverhøi, A., 1981. Evidence for a late Wisconsin glaciation of the Weddell Sea. *Nature*, 293:641-642.
- Elverhøi, A., and Roaldset, E., 1983. Glaciomarine sediments and suspended particulate matter, Weddell Sea Shelf, Antarctica. *Polar Res.*, 1:1-21.
- Emery, W. J., and Meincke, J., 1986. Global water masses: summary and review. *Oceanol. Acta*, 9:383-391.
- Fisher, R. L., Jantsch, M. Z., and Comer, R. L., 1982. *General Bathymetric Chart of the Oceans (GEBCO), Scale 1:10,000,000. 5-9*: Ottawa (Canadian Hydrographic Service).
- Foldvik, A., and Gammelsrød, T., 1988. Notes on Southern Ocean hydrography, sea-ice and bottom water formation. *Palaeogeogr., Palaeoclimatol., Palaeoecol.*, 67:3-17.
- Foldvik, A., Gammelsrød, T., and Tørresen, T., 1985. Circulation and water masses on the southern Weddell Sea Shelf. *Antarct. Res. Ser.*, 43:5-20.
- Folk, R. L., 1966. A review of grain-size parameters. *Sedimentology*, 6: 73-93.
- Folk, R. L., and Ward, W., 1957. Brazos River bar: a study in the significance of grain size parameters. *J. Sediment. Petrol.*, 27:3-26.
- Foster, T. D., and Carmack, E. C., 1976. Frontal Zone mixing and Antarctic Bottom Water formation in the southern Weddell Sea. *Deep-Sea Res.*, Part A, 23:294-301.
- Foster, T. D., Foldvik, A., and Middleton, J. H., 1987. Mixing and bottom water formation in the shelf break region of the southern Weddell Sea. *Deep-Sea Res.*, Part A, 34:1771-1794.
- Foster, T. D., and Middleton, J. H., 1979. Variability in the bottom water of the Weddell Sea. *Deep-Sea Res.*, Part A, 26:743-762.
- Fütterer, D. K., Grobe, H., and Grünig, S., 1988. Quaternary sediment patterns in the Weddell Sea: relations and environmental conditions. *Paleoceanography*, 3:551-561.
- Gordon, A. L., 1971. Antarctic Polar Front Zone. In Reid, V. L. (Ed.), *Antarctic Oceanology I*: Am. Geophys. Union Antarct. Res. Ser., 15:205-221.
- , 1978. Deep Antarctic convection west of Maud Rise. *J. Phys. Oceanogr.*, 8:600-612.
- , 1982. Weddell Deep Water variability. *J. Mar. Res.*, 40, Suppl.:199-217.
- Gordon, A. L., and Huber, B. A., 1984. Thermohaline stratification below the Southern Ocean sea ice. *J. Geophys. Res.*, 89:641-648.
- Griffin, J. J., Windom, H., and Goldberg, E. D., 1968. The distribution of clay minerals in the world ocean. *Deep-Sea Res.*, Part A, 15: 433-459.
- Grobe, H., 1986. *Spätpleistozäne Sedimentationsprozesse am antarktischen Kontinenthang vor Kapp Norvegia, östliche Weddell See*. Repts. Polar Res. 27.
- Grobe, H., Mackensen, A., Hubberten, H.-W., Spieß, V., and Fütterer, D. K., 1990. Stable isotope record and late Quaternary sedimentation rates at the Antarctic continental margin. In Bleil, U., and Thiede, J. (Eds.), *Geological History of Polar Oceans: Arctic versus Antarctic*. NATO/ASI Series C., Dordrecht (Kluwer Academic), 539-572.
- Hayes, D. E., and Vogel, M., 1981. *General Bathymetric Chart of the Oceans (GEBCO), Scale 1:10,000,000. 5-13*: Ottawa (Canadian Hydrographic Service).
- Hellmer, H. H., 1989. *Ein zweidimensionales Modell zur thermohalinen Zirkulation unter dem Schelfeis*. Repts. Polar Res., 60.
- Houtz, R. E., Hayes, D. E., and Markl, R. G., 1977. Kerguelen Plateau bathymetry, sediment distribution and crustal structure. *Mar. Geol.*, 25:95-130.
- Jacobs, S. S., Amos, A. F., and Bruchhausen, P. M., 1970. Ross Sea oceanography and Antarctic Bottom Water formation. *Deep-Sea Res.*, Part A, 17:935-962.
- Kellogg, T. B., and Kellogg, D. E., 1988. Antarctic cryogenic sediments: biotic and inorganic facies of ice shelf and marine-based ice sheet environments. *Palaeogeogr., Palaeoclimatol., Palaeoecol.*, 67:51-74.
- Kellogg, T. B., Truesdale, R. S., and Ostermann, L. E., 1979. Late Quaternary extent of the West Antarctic Ice Sheet: new evidence from Ross Sea cores. *Geology*, 7:249-253.
- Kennett, J. P., and Watkins, N. D., 1975. Deep-sea erosion and manganese nodule development in the southeast Indian Ocean. *Science*, 188:1011-1013.
- , 1976. Regional deep-sea dynamic processes recorded by late Cenozoic sediments of the southeastern Indian Ocean. *Geol. Soc. Am. Bull.*, 87:321-339.
- Killworth, P. D., 1979. On "chimney" formations in the ocean. *J. Phys. Oceanogr.*, 9:531-554.
- Kolla, V., Bé, A.W.H., and Biscaye, P. E., 1976a. Calcium carbonate distribution in the surface sediments of the Indian Ocean. *J. Geophys. Res.*, 81:2605-2616.
- Kolla, V., Sullivan, L., Streeter, S. S., and Langseth, M. G., 1976b. Spreading of Antarctic Bottom Water and its effects on the floor of

the Indian Ocean inferred from bottom-water potential temperature, turbidity, and sea-floor photography. *Mar. Geol.*, 21:171-189.

Lange, H., 1982. Distribution of chlorite and kaolinite in eastern Atlantic sediments off North Africa. *Sedimentology*, 29:427-432.

Leg 119 Scientific Party, 1988. Leg 119 studies climatic history. *Geotimes*, 33:14-16.

Pettijohn, E. J., 1975. *Sedimentary Rocks*: New York (Harper & Row).

Pettijohn, E. J., Potter, P. E., and Siever, R., 1987. *Sand and Sandstone* (2d ed.): New York (Springer-Verlag).

Pudsey, C. J., Barker, P. F., and Hamilton, N., 1988. Weddell Sea abyssal sediments: a record of Antarctic Bottom Water flow. *Mar. Geol.*, 81:289-314.

Van Andel, T. H., 1975. Mesozoic/Cenozoic calcite compensation depth and the global distribution of calcareous sediments. *Earth Planet. Sci. Lett.*, 26:187-194.

Vorren, T. O., Hald, M., and Lebesbye, E., 1988. Late Cenozoic environments in the Barents Sea. *Paleoceanography*, 3:601-612.

Whitworth, T., III, 1988. The Antarctic Circumpolar Current. *Oceanus*, 31:53-58.

Date of initial receipt: 11 September 1989

Date of acceptance: 2 February 1990

Ms 119B-123

Appendix Table 1. Sediment composition in an interval investigated in Hole 745B (Fig. 2).

Core, section, interval (cm)	Depth ^a (mbsf)	Opal (%)	Terrigenous material (%)	Organic carbon (%)	Carbonate (%)	Quartz (%)	Quartz/feldspar
119-745B-							
7H-2, 5-6	54.00	47.7	52.3	0.16	0.34	9.2	2.1
7H-2, 15-16	54.10	40.7	59.3	0.15	0.25	10.0	2.2
7H-2, 29-30	54.24	24.5	75.5	0.14	0.36	12.7	2.2
7H-2, 40-41	54.34	18.5	81.6	0.18	0.49	12.5	2.3
7H-2, 48-50	54.42	16.5	83.5	0.20	0.92	11.4	2.2
7H-2, 65-66	54.59	49.5	50.5	0.16	0.60	6.6	2.0
7H-2, 90-91	54.83	44.6	55.4	0.11	1.62	7.0	2.1
7H-2, 110-111	55.02	40.4	59.6	0.12	0.53	6.6	1.5
7H-2, 140-141	55.32	47.1	52.9	0.11	0.31	6.4	1.6
7H-3, 26-27	55.67	34.2	65.8	0.13	7.47	6.2	1.7
7H-3, 48-50	55.88	13.0	87.0	0.20	0.42	7.4	1.9
7H-3, 70-71	56.09	24.1	75.9	0.09	0.45	8.9	1.9
7H-3, 90-91	56.29	15.0	85.0	0.17	0.31	11.1	2.0
7H-3, 110-111	56.48	20.7	79.3	0.15	0.31	9.7	2.0
7H-3, 132-133	56.69	22.5	77.5	0.14	0.22	11.2	2.0
7H-4, 10-11	56.97	24.2	75.9	0.15	0.32	11.5	2.1
7H-4, 32-33	57.18	53.2	46.8	0.17	0.20	4.6	1.0
7H-4, 48-50	57.33	63.8	36.2	0.17	0.36	7.7	2.3
7H-4, 70-71	57.55	52.9	47.1	0.14	0.35	6.0	1.5
7H-4, 98-99	57.82	55.2	44.0	0.16	0.18	4.9	1.5
7H-4, 121-122	58.04	62.1	37.9	0.15	0.17	4.8	1.3
7H-4, 140-141	58.23	53.8	46.3	0.15	0.40	8.7	2.1
7H-5, 10-11	58.42	45.1	54.9	0.14	1.14	5.8	1.5
7H-5, 25-26	58.57	31.8	68.2	0.11	0.77	6.6	1.5
7H-5, 40-41	58.71	35.6	64.5	0.10	0.35	6.2	1.2
7H-5, 48-50	58.79	39.2	60.8	0.12	0.57	6.2	1.4
7H-5, 60-61	58.91			0.10	0.24	7.4	1.9
7H-5, 80-81	59.10	39.2	60.8	0.11	0.24	6.2	1.2
7H-5, 97-98	59.27	41.0	59.0	0.15	0.24	9.7	1.5

Note: Data are given in weight percent, except for quartz/feldspar in XRD peak-area ratios.

^a Corrected for recoveries >100%.

Appendix Table 2. Grain-size distribution of the bulk sediment and terrigenous and opaline components in an interval from Hole 745B (Fig. 3).

Core, section, interval (cm)	Depth (mbsf)	Bulk sediment				Opaline component			Terrigenous component		
		>2 mm (%)	63 μm-2 mm (%)	2-63 μm (%)	<2 μm (%)	63 μm-2 mm (%)	2-63 μm (%)	<2 μm (%)	63 μm-2 mm (%)	2-63 μm (%)	<2 μm (%)
119-745B-											
7H-2, 5-6	54.00	0.0	1.6	62.0	36.5	2.3	88.9	8.9	1.0	37.4	61.6
7H-2, 15-16	54.10	0.0	1.6	58.8	39.6	2.8	88.5	8.6	0.8	38.5	60.8
7H-2, 29-30	54.24	0.0	1.6	47.7	50.7	3.5	77.9	18.6	1.0	37.9	61.1
7H-2, 40-41	54.34	0.0	0.5	42.7	56.8	2.1	76.3	21.6	0.2	35.1	64.7
7H-2, 48-50	54.42	0.0	0.5	41.3	58.2	2.3	72.0	25.7	0.1	35.3	64.6
7H-2, 65-66	54.59	0.0	2.8	58.0	39.2	3.8	87.5	8.7	1.8	29.1	69.0
7H-2, 90-91	54.83	0.0	4.1	58.1	37.8	5.6	86.9	7.5	2.8	34.9	62.3
7H-2, 110-111	55.02	0.0	2.0	56.1	42.0	4.6	86.3	9.1	0.2	35.6	64.2
7H-2, 140-141	55.32	0.0	2.5	60.2	37.3	4.9	88.2	6.9	0.3	35.4	64.3
7H-3, 26-27	55.67	0.0	2.9	47.9	49.2	7.1	90.4	2.5	0.7	25.8	73.5
7H-3, 48-50	55.88	0.0	1.4	30.9	67.7	9.5	76.5	14.0	0.2	24.1	75.7
7H-3, 70-71	56.09	0.0	0.5	42.0	57.5	1.7	85.6	12.7	0.1	28.2	71.7
7H-3, 90-91	56.29	0.0	0.2	34.0	65.8	0.9	77.8	21.3	0.0	26.3	73.7
7H-3, 110-111	56.48	0.0	0.9	34.6	64.4	3.9	72.0	24.1	0.2	24.9	74.9
7H-3, 132-133	56.69	0.0	0.4	41.3	58.3	1.4	82.7	15.9	0.0	29.3	70.6
7H-4, 10-11	56.97	0.0	0.2	39.8	60.0	0.5	80.3	19.2	0.1	26.9	73.0
7H-4, 32-33	57.18	0.0	2.4	62.9	34.7	4.2	90.7	5.1	0.4	31.2	68.5
7H-4, 48-50	57.33	0.0	2.5	64.9	32.6	3.7	92.0	4.3	0.5	17.0	82.5
7H-4, 70-71	57.55	0.0	2.3	64.6	33.1	4.2	89.8	6.1	0.2	36.2	63.6
7H-4, 98-99	57.82	0.0	3.1	64.8	32.0	3.0	93.9	3.1	1.4	29.5	69.0
7H-4, 121-122	58.04	0.0	4.2	68.5	27.3	6.3	89.6	4.1	0.9	33.8	65.4
7H-4, 140-141	58.23	0.0	3.1	64.0	32.9	4.7	90.9	4.4	1.4	32.7	65.9
7H-5, 10-11	58.42	0.0	2.5	58.2	39.3	4.5	94.2	1.3	0.9	28.5	70.5
7H-5, 25-26	58.57	0.0	1.4	45.8	52.8	2.3	89.5	8.2	0.9	25.4	73.7
7H-5, 40-41	58.71	0.0	1.5	46.0	52.6	2.6	86.0	11.3	0.9	23.8	75.3
7H-5, 48-50	58.79	0.0	2.1	53.1	44.9	4.0	88.4	7.7	0.8	30.3	68.8
7H-5, 60-61	58.91	0.0	1.5	52.3	46.2						
7H-5, 80-81	59.10	0.0	1.9	55.7	42.5	4.5	87.6	7.9	0.2	35.1	64.7
7H-5, 97-98	59.27	0.0	1.7	56.8	41.4	4.0	89.1	6.9	0.2	34.4	65.4

Appendix Table 3. Statistical grain-size parameters (Folk and Ward, 1957; Folk, 1966) of the terrigenous material in an interval from Hole 745B (Fig. 4).

Core, section, interval (cm)	Depth (mbsf)	Mean (φ)	Median (φ)	Skewness	Kurtosis	Sorting (φ)
119-745B-						
7H-2, 5-6	54.00	9.4	10.0	-0.34	0.7	2.3
7H-2, 15-16	54.10	9.4	10.0	-0.34	0.7	2.3
7H-2, 29-30	54.24	9.5	10.0	-0.32	0.8	2.2
7H-2, 40-41	54.34	9.7	10.2	-0.32	0.8	2.0
7H-2, 48-50	54.42	9.8	10.1	-0.26	0.9	1.9
7H-2, 65-66	54.59	9.7	10.3	-0.40	0.9	2.2
7H-2, 90-91	54.83	9.3	10.0	-0.39	0.8	2.4
7H-2, 110-111	55.02	9.7	10.2	-0.35	0.8	2.1
7H-2, 140-141	55.32	9.6	10.1	-0.35	0.8	2.2
7H-3, 26-27	55.67	9.9	10.4	-0.39	1.1	2.0
7H-3, 48-50	55.88	10.1	10.4	-0.31	1.1	1.8
7H-3, 70-71	56.09	9.9	10.3	-0.30	1.0	1.9
7H-3, 90-91	56.29	10.0	10.4	-0.31	1.0	1.8
7H-3, 110-111	56.48	10.1	10.4	-0.30	1.0	1.8
7H-3, 132-133	56.69	9.9	10.3	-0.33	0.9	1.9
7H-4, 10-11	56.97	10.0	10.4	-0.31	1.0	1.8
7H-4, 32-33	57.18	9.6	10.3	-0.41	0.8	2.2
7H-4, 48-50	57.33	10.1	10.7	-0.48	1.6	2.1
7H-4, 70-71	57.55	9.4	10.2	-0.43	0.7	2.4
7H-4, 98-99	57.82	9.6	10.3	-0.43	0.9	2.3
7H-4, 121-122	58.04	9.3	10.2	-0.45	0.8	2.5
7H-4, 140-141	58.23	9.4	10.2	-0.44	0.8	2.5
7H-5, 10-11	58.42	9.7	10.3	-0.42	0.9	2.2
7H-5, 25-26	58.57	9.9	10.4	-0.39	1.1	2.1
7H-5, 40-41	58.71	9.9	10.5	-0.42	1.2	2.1
7H-5, 48-50	58.79	9.7	10.2	-0.35	1.0	2.1
7H-5, 60-61	58.91					
7H-5, 80-81	59.10	9.5	10.2	-0.41	0.8	2.3
7H-5, 97-98	59.27	9.5	10.2	-0.41	0.8	2.3

Appendix Table 4. Amount of terrigenous clay (nonbiogenic, <2 μm) and relative percentages of the clay minerals smectite, illite, chlorite, and kaolinite in an interval from Hole 745B (Fig. 5).

Core, section, interval (cm)	Depth (mbsf)	Clay (%)	Smectite (%)	Illite (%)	Chlorite (%)	Kaolinite (%)
119B-745B-						
7H-2, 5-6	54.00	32.2	14	63	20	3
7H-2, 15-16	54.10	36.1	17	65	10	8
7H-2, 29-30	54.24	46.1	11	54	19	16
7H-2, 40-41	54.34	52.8	11	62	12	15
7H-2, 48-50	54.42	54.0	14	63	5	17
7H-2, 65-66	54.59	34.8	21	62	8	9
7H-2, 90-91	54.83	34.5	22	63	10	5
7H-2, 110-111	55.02	38.3	28	55	12	5
7H-2, 140-141	55.32	34.1	28	55	7	10
7H-3, 26-27	55.67	48.4	16	59	18	8
7H-3, 48-50	55.88	65.9	21	54	17	8
7H-3, 70-71	56.09	54.4	24	56	13	7
7H-3, 90-91	56.29	62.6	11	60	19	10
7H-3, 110-111	56.48	59.5	14	66	13	7
7H-3, 132-133	56.69	54.8	20	57	18	5
7H-4, 10-11	56.97	55.4	19	62	11	8
7H-4, 32-33	57.18	32.1	44	48	3	5
7H-4, 48-50	57.33	29.8	35	44	21	0
7H-4, 70-71	57.55	29.9	33	52	12	4
7H-4, 98-99	57.82	30.3	45	36	11	8
7H-4, 121-122	58.04	24.8	11	69	20	0
7H-4, 140-141	58.23	30.5	17	65	10	8
7H-5, 10-11	58.42	38.7	13	60	12	15
7H-5, 25-26	58.57	50.2	19	63	11	8
7H-5, 40-41	58.71	48.5	15	70	9	7
7H-5, 48-50	58.79	41.9	20	56	13	10
7H-5, 60-61	58.91	41.9	34	53	7	6
7H-5, 80-81	59.10	39.4	33	50	11	6
7H-5, 97-98	59.27	38.6	29	57	6	8

Appendix Table 5. Concentration of quartz and feldspar (Fig. 6) by grain counts and roundness of quartz grains in the terrigenous sand fraction (63 μm -2 mm) in an interval from Hole 745B. Roundness classes according to Pettijohn (1975).

Core, section, interval (cm)	Depth (mbsf)	Number of grains	Composition (%)		Roundness (%)					
			Feldspar	Quartz	Angular	Subangular	Subrounded	Rounded	Well rounded	
119-745B-										
7H-2, 5-6	54.00	419	11.9	75.7	1.6	73.5	21.5	3.2	0.3	
7H-2, 15-16	54.10	435	10.8	79.3	5.2	69.6	24.0	0.8	0.3	
7H-2, 29-30	54.24	447	9.6	77.2	7.0	73.3	16.8	2.3	0.5	
7H-2, 40-41	54.34	475	9.9	64.4	5.2	67.0	25.8	2.0	0.0	
7H-2, 48-50	54.42	466	12.2	65.7	3.6	71.6	22.9	1.9	0.0	
7H-2, 65-66	54.59	426	14.3	73.5	12.1	69.0	16.0	2.6	0.3	
7H-2, 90-91	54.83	464	10.6	67.5	6.1	76.4	11.7	1.9	0.3	
7H-2, 110-111	55.02	163	16.6	74.8	5.7	56.6	22.1	14.8	0.8	
7H-2, 140-141	55.32	447	10.3	68.0	2.6	77.3	17.8	2.0	0.3	
7H-3, 26-27	55.67	423	15.8	68.3	7.3	70.6	19.4	2.4	0.4	
7H-3, 48-50	55.88	278	6.8	52.2	3.5	66.9	26.2	2.8	0.7	
7H-3, 70-71	56.09	275	11.3	70.2	1.6	67.4	29.0	2.1	0.0	
7H-3, 90-91	56.29	159	8.8	83.6	0.7	63.9	31.6	3.8	0.0	
7H-3, 110-111	56.48	351	7.4	80.1	2.9	68.7	25.3	2.1	1.1	
7H-3, 132-133	56.69	95	9.5	84.2	6.3	57.5	23.8	11.3	1.3	
7H-4, 10-11	56.97	230	19.6	74.3	7.0	67.8	21.7	3.5	0.0	
7H-4, 32-33	57.18	306	9.5	73.2	4.0	70.1	23.2	2.2	0.4	
7H-4, 48-50	57.33	427	4.7	19.4	9.6	66.3	22.8	1.2	0.0	
7H-4, 70-71	57.55	199	10.1	72.9	0.0	75.9	21.4	2.8	0.0	
7H-4, 98-99	57.82	424	13.9	72.9	0.6	66.3	30.4	2.6	0.0	
7H-4, 121-122	58.04	392	11.5	74.2	0.7	72.2	24.1	3.1	0.0	
7H-4, 140-141	58.23	422	6.6	80.6	3.2	66.2	27.9	2.4	0.3	
7H-5, 10-11	58.42	435	10.6	75.9	0.3	71.2	25.2	3.0	0.3	
7H-5, 25-26	58.57	429	13.5	73.4	2.9	74.6	22.2	0.3	0.0	
7H-5, 40-41	58.71	429	11.4	72.0	2.6	62.1	32.7	1.9	0.7	
7H-5, 48-50	58.79	436	11.7	73.4	2.5	80.9	15.0	1.6	0.0	
7H-5, 60-61	58.91	206	19.9	59.2	0.0	54.1	45.1	0.8	0.0	
7H-5, 80-81	59.10	313	8.3	78.9	3.6	73.7	20.2	2.4	0.0	
7H-5, 97-98	59.27	412	5.1	72.6	3.0	59.5	34.1	3.0	0.3	